Catalytic pre-coat on ceramic nanofiltration membranes for segregation and Fenton cleaning of high-resistance colloids in direct surface water treatment

Lin, Bin; Heijman, Sebastiaan G.J.; Rietveld, Luuk C.

Important note
To cite this publication, please use the final published version (if applicable).
Please check the document version above.

Catalytic pre-coat on ceramic nanofiltration membranes for segregation and Fenton cleaning of high-resistance colloids in direct surface water treatment

Bin Lin [a,b,*], Sebastiaan G.J. Heijman [a], Luuk C. Rietveld [a]

[a] *Department of Water Management, Faculty of Civil Engineering and Geosciences, Delft University of Technology, Stevinweg 1, 2628, CN Delft, the Netherlands*
[b] *State Key Laboratory of Materials-Oriented Chemical Engineering, National Engineering Research Center for Special Separation Membrane, Nanjing Tech University, Nanjing, 210009, China*

A B S T R A C T

Ceramic nanofiltration (NF) is a promising alternative for direct surface water treatment, but is hampered for full-scale applications by fouling and a lack of eco-friendly cleaning regimes. In this work, an innovative reactive pre-coat layer, consisting of an iron oxychloride catalyst, was constructed on top of commercial ceramic NF membranes, for segregating a large-sized colloid fraction in canal water and Fenton cleaning with a hydrogen peroxide (H_2O_2) solution. The large-sized colloids (3−30 μm) were identified as dominant substances fouling the TiO_2 separation layer of the pristine membranes, leading to a fast increase in their filtration resistance, in contrast to the small-sized colloids (<0.04 μm) and natural organic matter (NOM). As a consequence, the catalyst pre-coat layer with a pore size of 0.1–0.5 μm was able to segregate the large-sized colloids from the TiO_2 separation layer during direct filtration of the raw water. Moreover, filtration under an acceptable flux of around 23 L m^{-2} h^{-1} did not cause pore clogging in the catalyst pre-coat. In addition, Fenton oxidation initiated by the catalytic pre-coat efficiently restored the filtration resistance, whereas sole H_2O_2 flush of the pristine membrane was not effective. In the meantime, the TiO_2 separation layer of the membrane exerted a high NOM rejection of approximately 90%, measured as dissolved organic carbon, while the catalyst pre-coat on the membrane remained active in Fenton cleaning, over five one-day cycles. The findings of this work may provide guidance on the structural and functional design of a catalytic pre-coat layer for a dual purpose of foulant segregation and oxidative removal, particularly in response to key fouling-causing substances, during membrane-based treatment of real water matrices.

1. Introduction

Conventional drinking water treatment consists of multiple treatment units such as coagulation, flocculation, sedimentation, sand filtration and chlorination, resulting in a large footprint [1,2]. As a promising alternative, direct nanofiltration (NF) of surface water, without pre-treatment, aims to lower production costs and simplify the usual water processing train with a single-step, chemical-free operation [3]. However, most of the commercially available NF membranes, e.g. polymeric spiral-wound membranes, are susceptible to biofouling as a result of biological growth on the feed spacers, which cannot be cleaned by chlorine [4,5]. Alternatively, polyamide thin-film composite membranes can only be operated at a very low flux (e.g. 4 L m^{-2} h^{-1}) during

direct surface water treatment, in order to avoid frequent chemical cleaning and membrane replacement [6]. As reported currently, various ceramic (e.g. SiO_2, TiO_2 and TiO_2/ZrO_2) NF membranes [7] have shown smaller flux declines (<40%) during natural organic matter (NOM) fouling in constant pressure experiments, than polymeric ones (>70%) [8,9]. As biofouling grows rather slowly on ceramic NF membranes, cleaning of the membranes once a month with chlorine is able to prevent biofouling during surface water treatment. Hence, organic fouling remains the main fouling type, affecting the performance of ceramic NF membranes.

Apart from soluble NOM molecules, organic foulants in practical surface water are also present as colloidal matter [10,11]. Some researchers suggested that the coexistence of the two types of foulants

---

* Corresponding author. Department of Water Management, Faculty of Civil Engineering and Geosciences, Delft University of Technology, Stevinweg 1, 2628, CN Delft, the Netherlands.
  E-mail addresses: b.lin@tudelft.nl, binlin-1@outlook.com (B. Lin).

during membrane filtration could develop a more compact and firmly attached fouling layer on the membrane surface than the individual foulant alone [12–14]. There is also a study, however, demonstrating a smaller flux decline during combined NOM/colloidal fouling than obtained based on an additive sum of the individual contributions of NOM and colloidal fouling to flux declines [15]. There have been many studies focusing on NOM or colloidal fouling of ceramic NF membranes using model organic matter (e.g. humic acid, fulvic acid and meat peptone) [16,17] or colloids (e.g. Ca-alginate) [18], however, the overall fouling behaviour and cleanability of real NOM/colloid mixtures in surface water cannot be simply predicted from the principles regarding individual model foulants alone. Therefore, an understanding of the combined fouling and cleanability of ceramic NF membranes in relation to coexisting NOM and colloids, is of practical significance for the better design and development of direct surface water NF systems.

With respect to cleanability of model NOM or colloidal fouling over ceramic NF, Zhao et al. [7] and Mustafa et al. [16] reported that forward flush resulted in low flux recovery rates of 30–50%, due to the compact and sticky nature of the cake layer onto the separation layer of the membrane. In addition, it has been observed that hydraulic backwash can break the sealings at both ends of tubular ceramic NF membranes by a back-flow under high pressures [19]. As such, chemical cleaning with sodium hypochlorite (NaClO) [20,21] or caustic soda (NaOH)/citric acid [22] has to be frequently executed for effective flux restoration of TiO_2 and SiO_2 ceramic NF membranes, leading to a considerable increase in the defect percentages up to 16% or an enlargement of the membrane pores by 40–60% on a long-term basis. As an alternative, a catalyst-functionalized ceramic NF hybrid process is expected to enable the membrane to be cleaned through advanced oxidation processes with *in-situ* formed reactive oxygen species (e.g. hydroxyl and sulphate radicals) at the foulant-membrane interface. Current research about ceramic membrane-based oxidation (e.g. Fenton oxidation, peroxymonosulfate activation, catalytic ozonation and photocatalysis) has been exclusively focused on microfiltration and ultrafiltration, having different interface oxidation behaviour in relation to their specific fouling characteristics (e.g. internal adsorption and pore clogging) than that of NF [23–26]. To the best of our knowledge, oxidative cleaning in response to fouling development of catalytic ceramic NF membranes in direct surface water treatment has not been studied in present literature.

Surface modification of ceramic membranes with reactive catalysts is a common practice to endow the membranes with a catalytic oxidation ability. The focus of current studies has been mainly put on coating the outer and inner surfaces of ceramic membranes with a thin catalyst film [24,25,27]. As previously suggested, however, the surface Fenton reactions on thin iron-oxide film coated ceramic membranes suffered a considerable mass transfer hindrance, resulting from the formation of a thick and compact fouling layer on the membranes by sole NOM or NOM/colloid mixtures [23,28]. This is supposedly because the thin catalyst films, anchored on the membrane surfaces, lacked internal channels for the oxidant (i.e. H_2O_2) transportation, in particular when being covered and compacted with the fouling layer. Heredia Deba et al. demonstrated that the thicker TiO_2 layer (21.9 μm) on ceramic NF membranes, having more interconnected mass transfer channels, led to improved degradation of methylene blue (81%), compared to that (53%) by the thin TiO_2 film (0.3 μm) [29]. According to our recent work, the ceramic NF membrane, containing a porous iron-based catalyst layer (4.6 μm in thickness) on its surface, was able to restore the flux by over 90% after Fenton oxidation, notwithstanding a covering of alginate cake fouling on the catalyst layer [30]. Additionally, as demonstrated by Bai et al. [31,32], the Co–Al layered double hydroxide catalyst layer (>5 μm in thickness), coated on the surface of ceramic UF membranes, made a dominant contribution to oxidative de-fouling (69%) in contrast to the embedded Co-based oxide in the membrane pores (13%). However, the inner pores of the membranes were constricted by the embedded catalyst, while increasing the thickness of the externally coated catalytic layer (from 5 to 45 μm) did not cause a considerable increase in

permeance loss. Hence, rational design of a thick and porous catalyst layer on ceramic NF membranes, consisting of sufficient channels for water and oxidant transportation, may be a potential solution to mass transfer limitation caused by fouling, which calls for more research efforts.

Above all, the construction of a porous catalyst pre-coat layer on ceramic NF membranes needs to consider a dual purpose of segregating paramount foulants from the separation layer of the membranes and oxidative cleaning of the foulants via Fenton reactions at the pre-coat/foulant interface, during direct treatment of surface water characterized by heterogeneous NOM/colloid composition. To this end, in the present study, the heterogeneous Fenton catalyst, iron oxychloride (FeOCl) [33,34], was pre-coated on top of a commercial ceramic NF membrane, acting as both a pre-coat layer and a reactive catalytic layer. Herein, the catalyst coating was only performed on the membrane surface, where fouling was assumed to mostly take place, rather than within the membrane, to avoid blocking and constriction of the inner pores. The membranes with and without the reactive pre-coat layer were used to treat two different types of surface water: (i) untreated canal water containing a NOM/colloid mixture and (ii) canal water filtered through a 1.0-μm cartridge filter (to remove large-sized fractions of the colloids), in order to examine the effect of the pre-coat layer. Fouling behaviour of the membranes was studied in relation to the pre-coat layer, feed pH and permeate fluxes in a constant-flux filtration mode, to simulate as much as possible a potential full-scale application. The efficacy of separation and Fenton cleaning and the stability of the pre-coat layer were evaluated over multiple filtration and cleaning cycles.

2. Materials and methods

2.1. Surface water and membranes

Surface water was collected from the Delftse Schie Canal (Delft, the Netherlands), a moderately contaminated urban canal. The canal water had a dissolved organic carbon (DOC) concentration of 11.95 mg L^{-1} and a UV absorbance at 254 nm (UV_{254}) of 0.37 cm^{-1}. Other water quality parameters of the canal water are summarized in Table 1. The canal water was used: (i) as untreated for direct ceramic NF treatment, and (ii) after filtering through a 1.0-μm cartridge filter.

Commercial ceramic NF membranes (Inopor GmbH, Germany) with nominal molecular weight cut-off (MWCO) of 450 Da (Inopor data) were used in the experiments. As described by the manufacturer, the membranes have a single-channel tubular configuration with an effective filtration area of 0.00163 m^2 and an inner diameter of 7 mm. The membranes consist of a TiO_2 separation layer and an Al_2O_3 support layer. The virgin membranes were wetted by soaking in Milli-Q water (18.2 MΩ cm) overnight prior to use.

Table 1
Water quality parameters of Delftse Schie Canal water.

Parameters	Units	Values[a]
pH	/	8.55 ± 0.15
Turbidity	NTU	2.35 ± 0.05
DOC	mg L^{-1}	11.95 ± 0.13
UV_{254}	cm^{-1}	0.37 ± 0.01
Conductivity	mS cm^{-1}	2.42 ± 0.02
Ca^{2+}	mg L^{-1}	77.64 ± 0.14
Mg^{2+}	mg L^{-1}	17.71 ± 0.03
Na^+	mg L^{-1}	76.16 ± 0.57
K^+	mg L^{-1}	12.28 ± 0.14
PO_4^{3-}	mg L^{-1}	6.66 ± 0.04
SO_4^{2-}	mg L^{-1}	48.14 ± 0.44
Cl^-	mg L^{-1}	121.10 ± 0.38
Br^-	mg L^{-1}	1.84 ± 0.02

[a] Average ± SD from duplicate measurements.

2.2. Experimental methods

2.2.1. Coating of catalyst layer on ceramic NF membranes

A thermal annealing method was used to synthesize FeOCl catalyst [35]. The precursor, FeCl$_3$·6H$_2$O powder, was sealed in a crucible and calcined at a heating rate of 20 °C min^{-1} to 220 °C and remained for 1 h in a muffle furnace. The resultant FeOCl particles (2.0 g) were ultrasonically dispersed into demineralized water (0.5 L) and left to stand for 10 min to remove the settleable solids. The FeOCl suspension (Fig. S1a, Supplementary Data) remained stable and was thus favourable for pre-coating through pressure-driven pre-filtration, since undesirable sedimentation in the tubing could be avoided.

A crossflow filtration apparatus (OSMO Inspector 2, Convergence Industry, the Netherlands), with the FeOCl suspension (0.5 L) spiked into the feed mainstream (15 L), was used for membrane pre-coating (Fig. 1). The pre-coating experiments were performed in a pressure-driven crossflow filtration mode, because of its availability of a high transmembrane pressure (TMP) up to 20 bar and good applicability in full scale installations. A laminar cross flow of 0.2 m s^{-1} (Reynolds number (Re) = 1510, Text S1, Supplementary Data) and a high TMP of 9–20 bar were adopted to boost the formation of a uniformly compacted catalyst layer on the membrane. Two pristine membranes, having different permeance of 11.9 and 27.4 L m^{-2} h^{-1} bar^{-1}, were pre-coated at 20.2 and 8.9 bar, respectively, for 30 min, resulting in similar fluxes (233.9–234.8 L m^{-2} h^{-1}), to filter comparable amounts of the FeOCl catalyst onto the membranes. Additionally, the effect of FeOCl dosages (0–23.1 mg L^{-1}) in the feed flow on iron loading was studied by changing the flow rate with a peristaltic pump from the concentrated FeOCl tank (4.0 g L^{-1}), during pre-coating (10 min), also at comparable fluxes (213.3–220.3 L m^{-2} h^{-1}). The coating efficiency index (α) was calculated as a ratio of the actual loading (M_a, g m^{-2}) to the estimated loading (M_e, g m^{-2}), as described with Eq. (1).

$$\alpha = \frac{M_a}{M_e} = \frac{M_a}{C_{Fe} \bullet \int_0^t J_{Fe} dt} \tag{1}$$

where C_{Fe} (g L^{-1}) is the concentration of the FeOCl suspension in the feed flow, J_{Fe} (L m^{-2} h^{-1}) the temperature (20 °C) corrected permeate flux (Text S2, Supplementary Data) measured with the feed FeOCl suspension, and t (h) the operational time, during FeOCl pre-filtration. The actual FeOCl loading on the membranes was determined by dissolving the solid iron into an oxalic acid solution (1.0 g L^{-1}) and measuring the dissolved iron concentration, while the estimated FeOCl loading was calculated based on a mass balance of FeOCl filtered by the membranes.
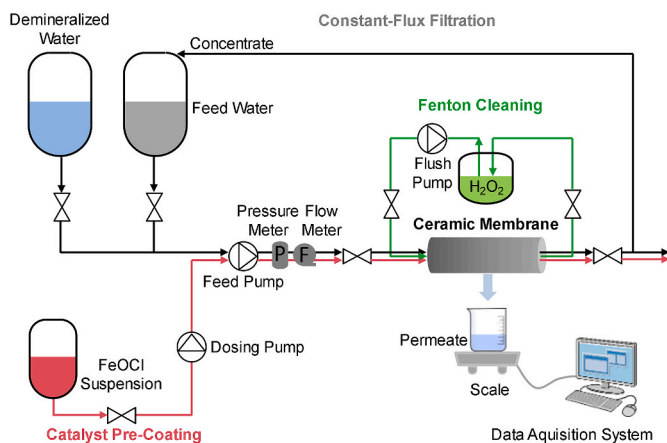

Fig. 1. Schematic diagram of the integrative system of catalyst layer coating, constant-flux filtration and Fenton cleaning for direct ceramic nanofiltration of surface water.

The pure water permeance of the membranes before and after precoating was measured at a constant TMP of 6–7 bar to determine the permeance loss.

2.2.2. Constant-flux filtration experiments of surface water and Fenton cleaning

Bench-scale filtration experiments were performed using the same crossflow filtration setup as the pre-coating tests (Fig. 1). The membranes with and without the pre-coat layer were tested with demineralized water to determine their initial filtration resistance. Direct NF experiments of the raw canal water (without any pre-treatment) were done in a constant-flux filtration mode through a step-wise increase in TMP (3–22 bar), in order to simulate as much as possible a full-scale application. The crossflow velocity was set at 0.9 m s^{-1} to acquire a turbulent flow (Re = 6039) inside the membrane channel, whereby organic fouling and concentration polarization on the membrane surface could be minimized as much as possible. The retentate flow was fed back into the feed tank, while the permeate flux was continuously measured using a scale connected to a data acquisition system. A NaClO solution (0.2%) was employed to ensure sufficient cleaning of the fouled membranes with and without the catalytic pre-coat layer after each test. An overview of the performed fouling and cleaning experiments is given in Table S1 (Supplementary Data). The filtration and cleaning experiments were done in duplicate.

2.2.2.1. Single-cycle fouling.
Single-cycle fouling (4 h) of the pristine and pre-coated ceramic NF membranes was evaluated at fluxes of around 23 and 46 L m^{-2} h^{-1}, respectively, which were set comparable to or higher than the operating fluxes adopted in direct surface water treatment using polyamide thin-film composite NF membranes (4 L m^{-2} h^{-1}) [6] and capillary NF membranes (27 L m^{-2} h^{-1}) [36]. Feed pH is an important factor affecting surface interactions (e.g. electrostatic interactions and calcium bridging) between membranes and foulants [37]. The raw water was subjected to the fouling tests at its original pH (8.5, Table 1) and also at pH = 7.0 (adjusted by a HCl solution of 1.0 M) to gain an insight into the fouling mechanism, since natural surface water typically has a pH value falling within the range of 7.0–8.5 [38–40]. In addition, to study the effect of colloids in the feed water on filtration, prefiltered canal water, over a 1.0-μm cartridge filter, was also subjected to the same ceramic NF operations as was the raw water.

2.2.2.2. Multi-cycle fouling and cleaning.
The efficacy of Fenton cleaning for the catalyst layer coated membrane, in comparison with that of sole hydrogen peroxide (H$_2$O$_2$) cleaning for the pristine membrane, was assessed during repeated constant-flux filtration and cleaning over five cycles (4-h fouling for each cycle). Membrane cleaning (30 min) was carried out by circulating a H$_2$O$_2$ solution ([H$_2$O$_2$]$_0$ = 10.0 mM; pH = 3.3) inside the membrane channel with a peristaltic pump at a laminar cross flow of 0.16 m s^{-1} (Re = 1116) as depicted in Fig. 1. A longer-term filtration and Fenton cleaning experiment over five cycles (1-d fouling for each cycle), was conducted in a constant-TMP filtration mode. The cleaning agent, i.e. H$_2$O$_2$ solution ([H$_2$O$_2$]$_0$ = 30.0 mM; pH = 3.3), was repeatedly used throughout the five one-day cycles, to evaluate the stability and sustainability of the Fenton cleaning route.

2.2.3. Membrane adsorption experiments

In order to study the fouling potential and mechanism with respect to foulant-membrane interactions, separate adsorption experiments were performed at TMP = 0 bar, meaning that there was no permeate flow with a closed permeate outlet. Initial fluxes of the pristine and precoated membranes were measured with demineralized water at a constant TMP of 6–7 bar, to establish a baseline permeance prior to adsorption. The demineralized water in the filtration setup was fully replaced with the canal water samples before the start of the adsorption experiments. Adsorption of NOM and colloids of the canal water onto

the membranes was then started by circulating the canal water inside the feed channel, using the same filtration setup and crossflow velocity (i.e. 0.9 m s^{-1}) as the filtration experiments, except without allowing a permeate flow (TMP = 0 bar). The adsorption tests were conducted at the original feed pH (8.5, Table 1) and at pH = 7.0 at 20 °C, to better understand the underlying adsorption mechanisms. An adsorption duration of 5 min was adopted to evaluate the potential of rapid adsorption of the foulants on and in the membranes. After adsorption, the feed water was finally switched back to demineralized water to determine fluxes at the same TMP (6–7 bar) as used before adsorption. The contribution to declines in the pure water fluxes before and after adsorption was supposed to be adsorptive fouling, since cake layers are not able to build up in the absence of a permeate flow [41].

2.3. Model analysis

2.3.1. Determination of hydraulic filtration resistance

The hydraulic filtration resistance was determined using the resistance-in-series model [42] as described in Text S3 (Supplementary Data). The resistance at the varying filtration conditions and stages was calculated as follows:

$$R_m = \frac{\Delta P_1}{\eta \bullet J_1} \tag{2}$$

$$R_m + R_{pc} = \frac{\Delta P_1}{\eta \bullet J_2} \tag{3}$$

$$R = R_m + R_{pc} + R_f = \frac{\Delta P}{\eta \bullet J} \tag{4}$$

where R_m (m^{-1}), R_{pc} (m^{-1}), R_f (m^{-1}) and R (m^{-1}) are the filtration resistance of the pristine membrane, pre-coat layer and fouling layer, and the total filtration resistance, respectively. ΔP_1 (Pa) is the applied TMP during pure water filtration over both the pristine membrane and the pre-coated membrane, respectively, ΔP (Pa) the applied TMP during filtration with the canal water using the pre-coated (or pristine) membrane. J_1 (m s^{-1}) and J_2 (m s^{-1}) represent the pure water fluxes before and after FeOCl pre-coating, respectively, J (m s^{-1}) the permeate flux of the pre-coated (or pristine) membrane during filtration with the canal water, η (Pa s) the permeate viscosity.

2.3.2. Fouling mechanism analysis by constant-flux crossflow blocking laws

Fouling mechanisms during the constant-flux crossflow filtration experiments were identified using a combined intermediate pore blocking and cake filtration model proposed by Kirschner et al. [43]. The total filtration resistance during the progression of fouling was plotted as a function of the permeate volume per unit filtration area (V_s, m), and fitted to the combined model, as described in Eq. (5):

$$R = \frac{R_0 \bullet (1 + K_c \bullet V_s)}{\frac{1}{K_i} + \left(1 - \frac{1}{K_i}\right) \bullet e^{-\frac{K_i \bullet B}{J} \bullet V_s}} \tag{5}$$

where R_0 (m^{-1}) is the initial total filtration resistance, K_c (m^{-1}) the cake filtration constant, K_i the intermediate pore blocking constant, B (s^{-1}) the foulant detachment rate signifying the extent to which foulants are removed from a membrane surface by crossflow shear forces. The combined model was derived from the classical dead-end filtration blocking laws (i.e. complete pore blocking, intermediate pore blocking, standard pore blocking, and cake filtration) by incorporating a crossflow foulant removal term. In intermediate pore blocking, foulants incline to either block an open pore of membranes or deposit on a previously deposited foulant, whereby the probability of blocking of the open pores by the foulants decreases as an increased number of pores are blocked. Hence, the intermediate pore blocking law, used in the combined model, was in accordance with the constant-flux filtration condition.

Nevertheless, the complete and standard pore blocking laws with assuming progressive blocking of pore openings and inner pore walls, respectively, are not realistic to result in a constant flux, which were thus not incorporated into the combined model. Therefore, the combined model, used in this work, was based on the assumption that fouling in the constant-flux filtration mode occurs with partial blocking of the membrane pores followed by cake filtration.

2.4. Characterization and analytical methods

The DOC of the canal water was analysed by a total organic carbon analyser (TOC-VCPH, Shimadzu, Japan). The anions and cations in the canal water were measured with ion chromatography (883 Basic IC plus, Metrohm Instrument, the Netherlands). The UV$_{254}$ was determined by a UV/vis spectrometer (GENESYS 10S UV–Vis, Thermo Scientific, USA) with a quartz cell (1 cm). Prior to all the analyses, the water samples were filtrated through 0.45 μm filters to retain potential impurities. No significant difference in the dissolved water quality parameters was observed between the raw and 1.0-μm filter pre-treated canal water samples in our preliminary experiments (data not shown), due to the water sample preparation over the 0.45 μm filters. Therefore, we did not separately measure the dissolved water quality parameters for the 1.0 μm filter treated canal water.

The crystalline profiles of the FeOCl catalyst and the membranes before and after pre-coating were analysed between 5° and 60°, respectively, with a scan step of 0.3° min^{-1} by X-ray diffractometer (D8-Advance, Bruker, USA) under Cu Kα radiation at 45 kV and 40 mA. The contact angles of the pristine and pre-coated membranes were measured by an optical contact angle goniometer (SCA20, Dataphysics, Germany). The zeta potentials of the canal water samples and FeOCl suspensions (0.37 mM) were recorded using a NanoSizer (Nano Series, Malvern Instrument Ltd., UK). The top-view and cross-sectional mapping of the membranes before and after FeOCl pre-coating was taken by scanning electron microscopy (SEM) (S-3400 N, Hitachi High-Technologies, Japan), equipped with energy dispersive spectroscopy. The top surface and thickness of the remaining FeOCl pre-coat layer on the membrane, after the long-term (5 d) multicycle filtration and cleaning, were analysed with the SEM. The average roughness R_a (an arithmetic average of the profile height deviations from the mean plane) and the root mean square roughness R_q (a root mean square average of the profile height deviations from the mean plane) of the membranes, were measured by atomic force microscopy (AFM) (Dimension FastScan, Bruker, USA).

The actual MWCO of the membranes was determined by measuring the rejection rates of polyethylene glycols (PEGs) of five molecular weights (200, 300, 400, 600 and 1000 Da) (Sigma-Aldrich, Germany) as tracer compounds, as reported by Shang et al. [44]. The PEG samples were analysed by high-performance size exclusion chromatography (Prominence, Shimadzu, Japan), installed with a gel permeation column (5 mm 30 Å, PSS GmbH, Germany) and a refractive index detector (RID-20A, Shimadzu, Japan).

3. Results and discussion

3.1. Characterization of surface water, FeOCl catalyst and membranes

3.1.1. Colloidal sizes and charge properties of surface water

Ceramic NF membranes have abundant porous channels and charged surfaces, and are supposed to intercept large-sized or charged substances via steric hindrance and electrostatic repulsion, respectively [7,45]. Fig. 2a shows that the colloidal substances, present in the canal water, were characterized by a bimodal distribution of particle sizes in the range of <0.04 μm and 3–30 μm. The zeta potential profiles (Fig. 2b) imply that the NOM and colloids in the canal water were (mostly) negatively charged at pH = 6–9, because particles in surface water adsorb negatively charged humic acids [46]. The zeta potential of the solution was rather stable, ranging from −15.1 to −16.5 mV, as a
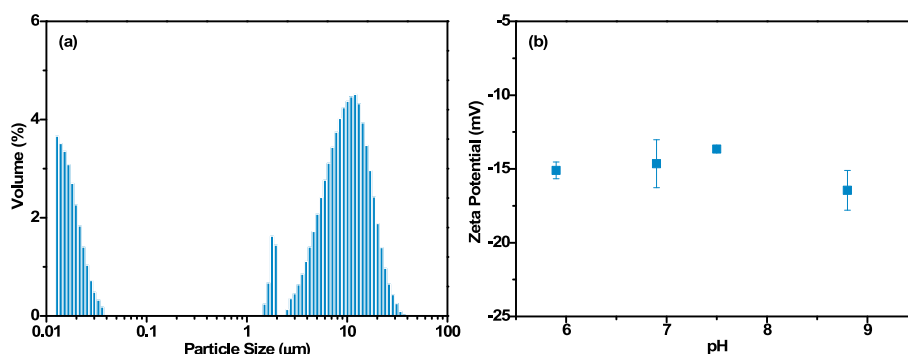
Fig. 2. (a) Colloidal size distribution and (b) zeta potential of canal water foulants.

function of the pH (6−9). Apparently, the NOM in the canal water was fully deprotonated above pH = 6.0, since pKa values of the predominant humic/fulvic acid carboxylic groups center around 4.7 and 5.9 [47].

3.1.2. FeOCl catalyst pre-coat layer and membranes

As measured in Fig. S2 (Supplementary Data), the FeOCl catalyst and FeOCl pre-coated membrane both presented standard characteristic crystalline phases, i.e. (010), (110), (021) and (111) planes, which are typical of pure-phase FeOCl (JCPDS No. 72–0619) [35]. As can be observed from Fig. 3a, the surface of the membrane channel changed from white to homogeneously brownish yellow, upon FeOCl pre-coating, meaning successful loading of the FeOCl catalyst onto the membrane. The pristine membrane exhibited a dense and smooth surface (Fig. 3b and c) of the TiO$_2$ separation layer, having low surface roughness of R_a = 3.25 nm and R_q = 4.13 nm (Table S2, Supplementary Data) as indicated by the AFM measurements. The pre-coated membrane, however, displayed a rougher surface (R_a = 21.67 nm; R_q = 28.97 nm), with the FeOCl particles randomly stacked on the membrane (Fig. 3d). Additionally, the FeOCl pre-coat layer enhanced surface hydrophobicity of the membrane, as suggested by the larger water contact angle of the pre-coated membrane (109.0°) compared to the pristine membrane (54.4°) (Table S2, Supplementary Data).

The FeOCl particles were present as long-strip sheets with dimensions of, approximately, 0.2−0.3 μm in thickness, 0.7−1.2 μm in width and 3.0−5.0 μm in length (Fig. S1b, Supplementary Data), which enabled the particles to deposit onto the membrane, instead of penetrating into the nano-pores (around 1 nm in diameter). The FeOCl layer had a pore size of 0.1–0.5 μm, as estimated from the top-view SEM image (Fig. 3d). Therefore, the FeOCl layer was assumed to act as a pre-filter media to retain the large-sized fraction (3–30 μm, Fig. 2a) of the colloids from the canal water, while only allowing the small-sized colloid fraction (<0.04 μm, Fig. 2a) and the dissolved molecules to pass through and reach the surface of the TiO$_2$ separation layer [48,49]. The pre-coat layer of about 5.3 μm in thickness (Fig. 3e), appeared to be uniformly coated on the membrane. As indicated by the PEG rejection curve in Fig. 3f, the measured MWCO of the membrane, i.e. 701 Da, was larger than the nominal MWCO (450 Da, Inopor data), as has also been observed in other studies on similar membranes [45,50,51]. The profile of zeta potential as a function of pH of the FeOCl suspension (Fig. S1c, Supplementary Data) showed an isoelectric point between pH = 7.0 and 8.1, corresponding to a positively charged surface of the FeOCl particles at pH = 7.0.

In order to test the adjustability of catalyst loading by means of crossflow pre-filtration, loading of the FeOCl particles was studied in
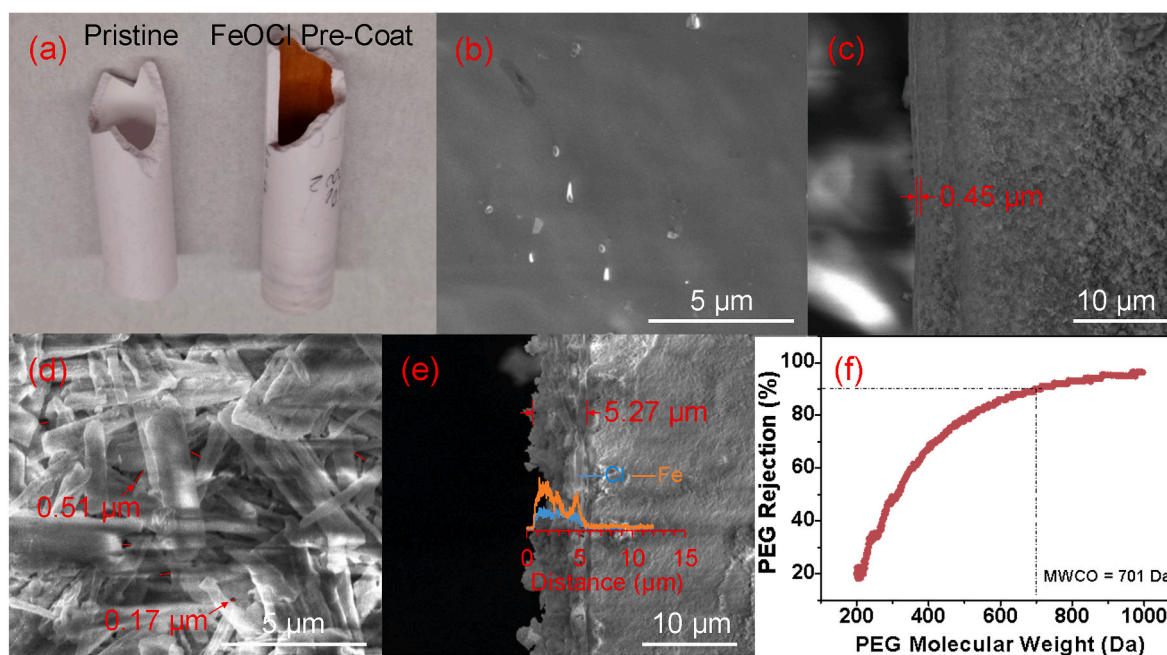

Fig. 3. (a) Photographs of pristine (left) and FeOCl pre-coated (right) ceramic NF membranes. (b) Top-view and (c) cross-section SEM images of pristine membrane. (d) Top-view and (e) cross-section SEM images with inset energy dispersive spectroscopy profiles of FeOCl pre-coated membrane. (f) Polyethylene glycol (PEG) rejection curve of ceramic NF membrane. The dashed line shows the PEG molecular weight with a rejection rate of 90%, representing the MWCO.

relation to different permeance (11.9 and 27.4 L m^{-2} h^{-1} bar^{-1}) of two pristine membranes and varying FeOCl dosages (0–23.1 mg L^{-1}). Fig. 4a depicts that the two membranes, when pre-coated at the similar fluxes (see Section 2.2.1), presented comparable FeOCl loading, being 2.7 and 2.4 g m^{-2}, respectively. This thus implies that maintaining the permeate flux at a certain level by tuning the TMP during pre-coating, is a viable method for obtaining the intended catalyst loading on the membranes. The actual loading of the membranes was less than a half (α < 46.0%, inset of Fig. 4a) of the theoretical loading (5.8–5.9 g m^{-2}), being the total amount of FeOCl filtered by the membranes. It is likely that the cross flow in the membrane channel limited the build-up of the FeOCl pre-coat layer on the membranes, due to a shear-induced diffusion effect [52]. The FeOCl loading on the membrane increased as a function of the FeOCl dosages, indicating that the FeOCl loading could also be regulated by changing the FeOCl dosages (Fig. 4b). The permeance losses of the membranes, as a result of FeOCl pre-coating, were minimal (<4%, inset of Fig. 4b). This is supposedly because the porous pre-coat layer provided alternative, interconnected channels for water permeation, since intraparticle micropores and particle interspaces (meso/macropores) were abundant in and between the FeOCl particles [35,53].

3.2. Fouling mechanism analysis with combined intermediate pore blocking and cake filtration model

Direct ceramic NF of raw canal water (Fig. 5a and b) was performed at its original pH (8.5) and at pH = 7.0, using the pristine and pre-coated membranes at a constant flux of 44.7–46.0 L m^{-2} h^{-1}, during a single filtration cycle, to elucidate the underlying fouling mechanisms and influential factors. The variations of each filtration resistance as a function of the volume per unit area, were well fitted to the combined intermediate pore blocking and cake filtration model (R^2 = 0.93–0.98) under the various conditions. The result indicates that the sharp increases in the initial filtration resistance, and afterwards the abrupt transition to the slower resistance increases, were ascribed to intermediate pore blocking and cake filtration, respectively. The model assumption (Section 2.3.2) suggests that the colloids and NOM, already adhered on the membrane surfaces, could hinder further blocking of the rest of the pore openings in nearby areas by the subsequently approaching foulants, thereby leading to a plateau of pore blocking and a transition to cake build-up. As shown in Table 2, both membranes presented larger intermediate pore blocking and cake filtration constants at pH = 8.5 (K_i = 3.08–3.22; K_c = 5.96–9.95 m^{-1}) than at pH = 7.0 (K_i = 2.44–2.46; K_c = 3.22–5.05 m^{-1}), which is presumably a result of increased calcium bridging between the membranes and foulants and between the foulants at the higher pH as suggested in prior studies with

consistent findings [17,37]. In addition, the pre-coated membrane exhibited slightly larger intermediate pore blocking constants (K_i = 2.44–3.22 versus 2.46–3.08) and much larger cake filtration constants (K_c = 5.05–9.95 versus 3.22–5.96 m^{-1}), compared to the pristine membrane. These observations would be further explained in relation to the influence of foulant sizes, permeation fluxes and adsorption affinities of the pristine and pre-coated membranes in the following discussion.

The effect of foulant sizes on filtration resistance was studied using the pre-filtered canal water for filtration of the pristine and pre-coated membranes at a constant flux of 45.9–47.5 L m^{-2} h^{-1} (Fig. 5c). As the raw water colloids had sizes of <0.04 μm and 3–30 μm (Fig. 2a), the pre-filtered canal water through a 1-μm filter was therefore assumed to only consist of a small-sized fraction of the colloids (<0.04 μm) and dissolved NOM. The pre-coated membrane developed a cake filtration constant (K_c = 1.92 m^{-1}) comparable to that of the pristine membrane (K_c = 2.22 m^{-1}), when filtering the pre-filtered canal water. This result implies that the formation of cake layer fouling by the small-sized colloid fraction and NOM was independent of the presence of the pre-coat layer. It is likely that the small foulants tended to penetrate the pre-coat layer and predominantly fouled the TiO$_2$ separation layer [48,54]. The result, however, largely differs from the observations during direct raw water (pH = 8.5) filtration in Fig. 5a and b, where the cake filtration constant of the pre-coated membrane was around 1.7 times that of the pristine membrane. Herein, the faster fouling during direct raw water filtration of the pre-coated membrane was supposedly because the large-sized fraction of the colloids filled and clogged the pores in the pre-coat layer, which was driven by a large permeation drag force at the flux of 44.7–46.0 L m^{-2} h^{-1}. The cake filtration constant (K_c = 1.92 m^{-1}) for filtration with the pre-filtered canal water (Fig. 5c), accounted for only 19.3% of that for filtration with the raw canal water (pH = 8.5) both using the pre-coated membrane (Fig. 5b), confirming the dominant role of the large-sized colloid fraction in clogging of the pre-coat layer driven by the high permeation fluxes.

To study the underlying influence of permeation fluxes on fouling of the pristine and pre-coated membranes, Fig. 5d illustrates the resistance evolution of the membranes during direct NF of the raw canal water at a constant flux of 22.8–23.1 L m^{-2} h^{-1}. Apparently, the pre-coated membrane underwent a little faster initial intermediate pore blocking (K_i = 3.26) than the pristine membrane (K_i = 3.06), but subsequently developed slower cake layer fouling (K_c = 5.94 m^{-1}), compared to the pristine membrane (K_c = 8.74 m^{-1}) at the flux of about 23 L m^{-2} h^{-1}. The result suggests that the pre-coat layer on the membrane during direct raw water NF at approximately 23 L m^{-2} h^{-1}, could segregate the large-sized colloid fraction from the TiO$_2$ separation layer without an occurrence of considerable clogging within itself, in contrast to the situation at around 46 L m^{-2} h^{-1}. This is mainly because the number of
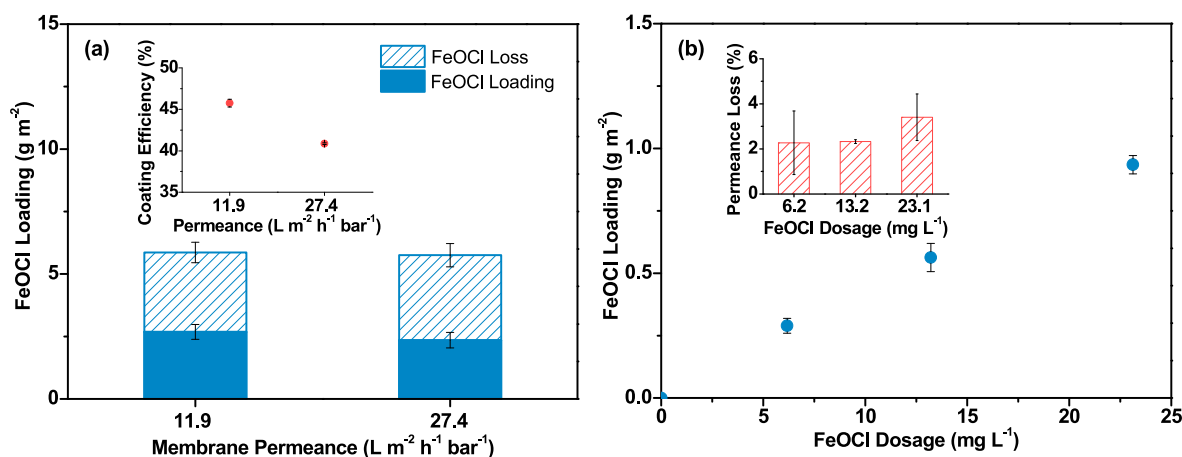

Fig. 4. (a) FeOCl loading of ceramic NF membranes with different initial permeance. Inset: FeOCl coating efficiency vs. membrane permeance. (b) Effect of FeOCl dosage on iron loading and permeance loss of ceramic NF membrane.
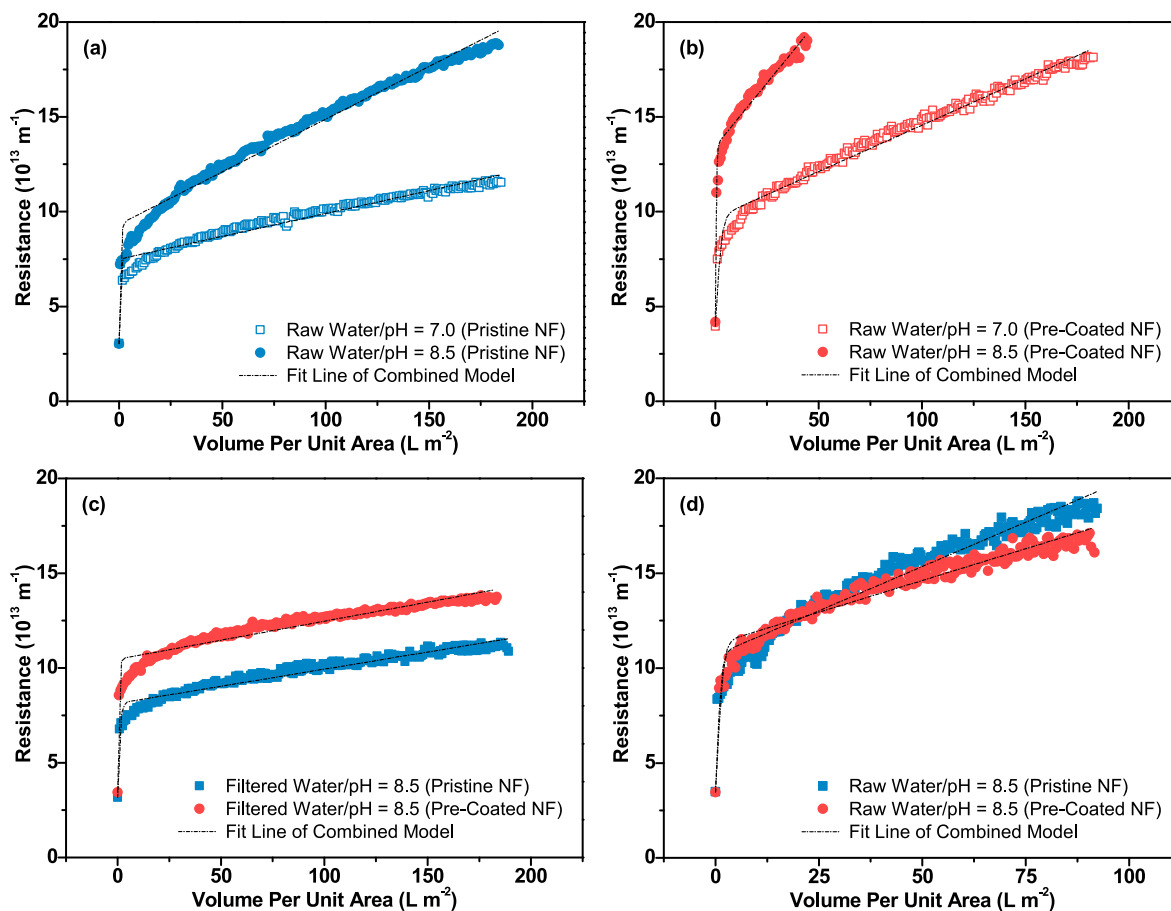
Fig. 5. Filtration resistance of (a) pristine and (b) FeOCl pre-coated membranes during direct NF of raw canal water at its original pH (8.5) and pH = 7.0, (c) during NF with pre-filtered canal water (by 1 μm cartridge filter) at pH = 8.5, at constant fluxes of around 46.0 L m^{-2} h^{-1}, and (d) during direct NF of raw canal water (pH = 8.5) at constant fluxes of about 23.0 L m^{-2} h^{-1}. The dashed curves correspond to the fitting of the filtration resistance variations to the combined intermediate pore blocking and cake filtration model.

Table 2
Fitting parameters of constant-flux crossflow combined intermediate pore blocking-cake filtration model.

Figure no.	Experimental conditions				Model fitting parameters			
	Membranes	Water types	Feed pH	J (L m^{-2} h^{-1})	K_c (m^{-1})	K_i	B (s^{-1})	R^2
Fig. 5a	Pristine NF	Raw water	7.0	45.9	3.22	2.46	0.0316	0.96
Fig. 5a	Pristine NF	Raw water	8.5	45.9	5.96	3.08	0.0105	0.98
Fig. 5b	Coated NF	Raw water	7.0	45.4	5.05	2.44	0.0038	0.98
Fig. 5b	Coated NF	Raw water	8.5	44.6	9.95	3.22	0.0131	0.97
Fig. 5c	Pristine NF	Filtered water	8.5	47.4	2.22	2.56	0.0085	0.95
Fig. 5c	Coated NF	Filtered water	8.5	45.8	1.92	3.04	0.0115	0.93
Fig. 5d	Pristine NF	Raw water	8.5	23.0	8.74	3.06	0.0038	0.95
Fig. 5d	Coated NF	Raw water	8.5	22.7	5.94	3.26	0.0028	0.95

foulants, carried by the lower flux, were fewer, compared to the higher flux, whereby the foulants might be well dispersed on and within the porous pre-coat layer without causing pronounced clogging of the pores [55]. In addition, it is likely that the cross flow (0.9 m s^{-1}) at the lower flux (with a weaker permeation drag force) could, to some extent, prevent the large-sized colloid fraction from entering the pores of the pre-coat layer.

3.3. Adsorptive fouling as a mechanism for initial sharp resistance increases

Adsorptive fouling identification, using the adsorption experiments (5 min) without a permeate flow through the membranes (Section 2.2.3), could provide an insight into the foulant-membrane interactions

at the very beginning of filtration with the raw canal water [56,57]. Fig. 6a shows that the flux decline of the pristine membrane upon adsorption at pH = 7.0 (19.7%) was much smaller than at pH = 8.5 (31.0%). The same tendency was observed for the FeOCl pre-coated membrane (Fig. 6b), where the flux decline due to adsorption at pH = 7.0 (30.7%) was also smaller than at pH = 8.5 (41.0%). These findings are in line with the observation of Kim et al. [37], who have demonstrated that the adsorption capacity of NOM (10 mg L^{-1}) onto TiO$_2$ particles was increased from 12 to 19 mg g^{-1} with an increase in the solution pH from 5 to 8. They have suggested that NOM-TiO$_2$ bridging by calcium ions (1 mM) was more prone to occur at pH = 8, where the TiO$_2$ surfaces were more negatively charged, than at pH = 5. Both membranes developed a progressive increase in the fluxes during pure water filtration after adsorption, implying that the adsorbed foulants
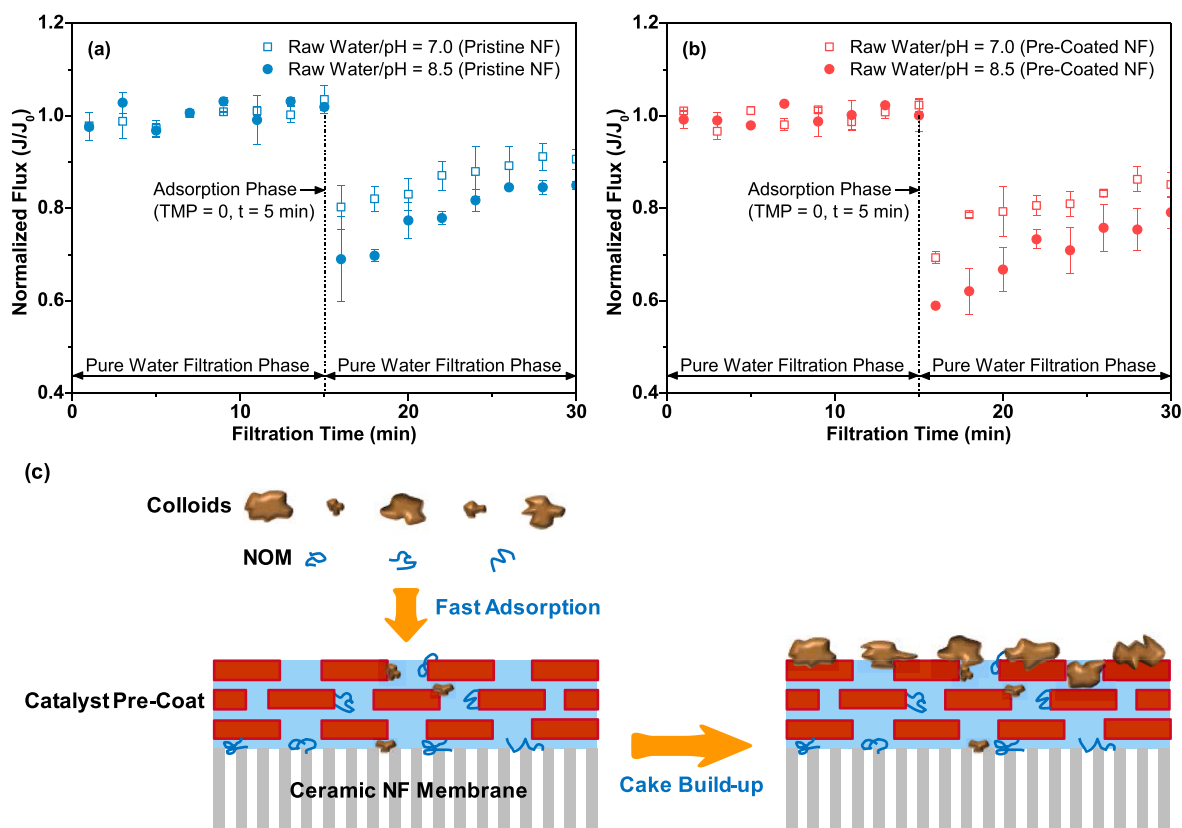
Fig. 6. Membrane permeance declines due to adsorption (5 min) of foulants from raw canal water to (a) pristine and (b) FeOCl pre-coated membranes at original (pH = 8.5) and neutral pH (7.0) of the canal water. (c) A schematic diagram of fouling development during a filtration period of canal water.

inclined to be desorbed to some extent during crossflow filtration with pure water.

Notably, the permeance declines during adsorption at the four combined conditions, well corresponded to the initial sharp increases of the filtration resistance observed in the single cycle filtration experiments (Section 3.2). This confirms the important role of adsorption capabilities of the membranes in their fouling, in particular, at the very beginning of filtration with the raw surface water. Hence, the larger intermediate pore blocking constants of the pre-coated membrane compared to those of the pristine membrane (Table 2), as revealed by the combined model fitting in Section 3.2, were mainly attributed to faster adsorption of the foulants onto the pore openings of the TiO$_2$ separation layer of the pre-coated membrane. Once some of the membrane pores were clogged or narrowed by the adsorbed foulants, cake layers started to grow, thereby slowly increasing the resistance [43,58]. The fouling steps, involving initial rapid adsorption and subsequent progressive cake layer build-up, are shown schematically in Fig. 6c. As the pre-coated membrane underwent a smaller total filtration resistance (16.7×10^{13} m^{-1}), compared to the pristine one (18.4×10^{13} m^{-1}) at the flux of ~23 L m^{-2} h^{-1} (Fig. 5d), it is thus inferred that the catalytic pre-coat layer could mitigate the cake layer fouling, during cake filtration, rather than the intermediate pore blocking, during initial foulant adsorption.

3.4. Filtration and cleaning performance over multiple cycles

Direct filtration of canal water using pristine and FeOCl pre-coated membranes, and membrane cleaning with a H$_2$O$_2$ solution ([H$_2$O$_2$]$_0$ = 10.0 mM; pH = 3.3), were performed over five 4-h cycles, without refreshing the FeOCl pre-coat layer between the cycles. The fluxes were kept constant at 22.1−22.6 L m^{-2} h^{-1}, to facilitate segregation of the large-sized colloid fraction by the pre-coat layer while avoiding its pore

clogging, as demonstrated in Section 3.2. As shown in Fig. 7, the pristine membrane underwent a continuous increase in filtration resistance from 11.5×10^{13}−21.3×10^{13} (*Cycle 1*) to 18.6×10^{13}−28.9×10^{13} m^{-1} (*Cycle 5*), respectively, while crossflow flushing with the H$_2$O$_2$ solution was done after each filtration cycle. The result confirms the ineffective removal of the foulants using H$_2$O$_2$ cleaning in the absence of a catalytic pre-coat layer on the membrane. However, the filtration resistance of the pre-coated membrane only slightly increased at *Cycle 2*, i.e. from
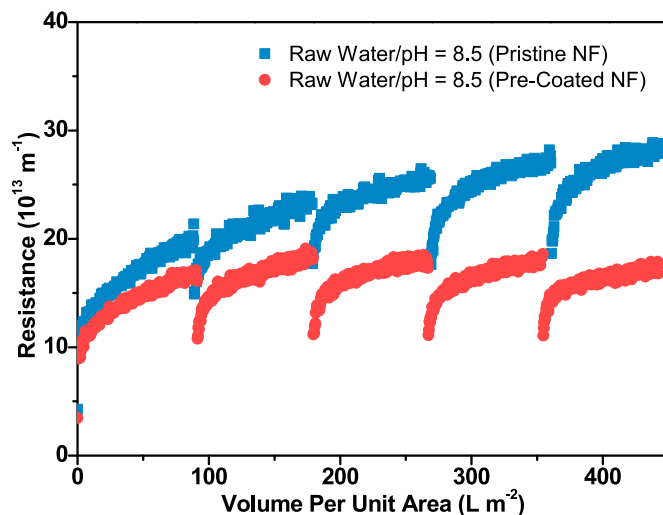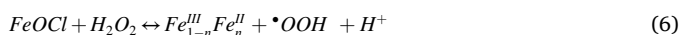

Fig. 7. Evolution of filtration resistance of pristine and FeOCl pre-coated membranes during direct filtration of raw canal water (pH = 8.5) at a constant flux of about 22.4 L m^{-2} h^{-1} and periodic H$_2$O$_2$ cleaning ([H$_2$O$_2$]$_0$ = 10.0 mM; pH = 3.3) over five 4-h cycles.

$8.9\times10^{13}-16.6\times10^{13}$ to $10.8\times10^{13}-18.4\times10^{13}$ m^{-1}, respectively, while, thereafter, it remained steady over the following cycles. The chemically irreversible fouling index (CIFI) (Text S4, Supplementary Data) of the pre-coated membrane was 0.00057 m^{-2} L^{-1}, accounting for less than 25% of the CIFI value of the pristine membrane (0.00231 m^{-2} L^{-1}) (Fig. S3, Supplementary Data). The majority of the foulants on and within the pre-coat layer, could be removed by Fenton oxidation re-actions catalysed by the FeOCl pre-coat layer as indicated in Eqs. (6) and (7) [34], avoiding aggressive cleaning with strong oxidants (e.g. NaClO) or bases (e.g. NaOH).

$$FeOCl + H_2O_2 \leftrightarrow Fe_{1-n}^{III}Fe_n^{II} + {}^{\bullet}OOH + H^+ \qquad (6)$$

$$\equiv Fe^{II} + H_2O_2 \leftrightarrow \equiv Fe^{III} + {}^{\bullet}OH + OH^- \qquad (7)$$

The coexistence of the Fenton catalyst (i.e. FeOCl), organic foulants (i.e. NOM and colloids) and H$_2$O$_2$ was favourable for degradation and removal of the foulants, due to a short mass transfer distance between ${}^{\bullet}$OH (hydroxyl radicals) and the foulants on and in the porous FeOCl pre-coat layer.

3.5. Validation of filtration performance of membranes and stability of catalytic pre-coat layer in long-running operations

The efficacy of separation and Fenton cleaning and the stability of the pre-coat layer during direct filtration of canal water, were further studied in a longer period of five one-day cycles. Constant-TMP filtration (TMP = 3.0 bar) was performed at an initial pure water flux of 21.7 L m^{-2} h^{-1} (Fig. S4, Supplementary Data), considering its ease in auto-matic regulation for continuous filtration, over days, at lab scale. As observed in Fig. S4, the pre-coated membrane experienced an abrupt flux decline by 42.5% at the very beginning of filtration, which was close to the flux decline percentage, i.e. 41.0% (Fig. 6b, Section 3.3), deter-mined by the adsorption experiment, and was thus assumed to pre-dominantly result from adsorption. Fig. 8a shows that the starting

resistance at *Cycle 2, 3* and *4* was recovered to a level as high as the one at *Cycle 1* following periodical Fenton cleaning, indicating effective removal of the foulants by Fenton cleaning. The multiple cycles pre-sented a gradually rising tendency in the overall filtration resistance with an increase in operation cycles, likely due to accumulation of some irremovable fouling during the longer filtration period (5 d) [59].

The rejection percentages of DOC, UV$_{254}$ and conductivity were recorded throughout the five filtration cycles of the canal water (Fig. 8b). The rejection percentages in DOC (87.7−89.9%) and UV$_{254}$ (88.0−89.4%) of the pre-coated membrane remained high and steady over the multiple cycles, almost the same as those of the pristine membrane (DOC rejection = 90.1%; UV$_{254}$ rejection = 89.7%), respec-tively, as shown in Table S3 (Supplementary Data). As a consequence, the removal of the dissolved organic molecules (i.e. NOM) was pre-dominantly ascribed to steric hindrance acted by the TiO$_2$ separation layer of the membrane [45]. Rejection of ions by ceramic NF mainly depends on electrostatic repulsion, since the sizes of the hydrated ions are much smaller than the pore sizes of the membrane (0.9 nm, Inopor data) [22,60]. As reported in two previous studies using the same ceramic NF membranes (Inopor GmbH, Germany) [61,62], the presence of multivalent counter ions (e.g. Mg^{2+} and Ca^{2+}) altered the zeta po-tential of the TiO$_2$ separation layer from $-40\sim-30$ to $-28\sim-20$ mV, respectively, indicating charge neutralization of the TiO$_2$ separation layer by the multivalent counter ions. As a result, the membrane un-derwent a progressive decrease in the ion rejection from 26.7% to 8.6% along with the five cycles, due to reduced electrostatic repulsion on the membrane surface upon exposure to the multivalent cations in the canal water ([Mg^{2+}] = 17.71 ± 0.03 mg L^{-1}; [Ca^{2+}] = 77.64 ± 0.14 mg L^{-1}, shown in Table 1). Defect percentages of the membrane over the repeated uses were regularly determined to ensure its good integrity. The membrane, after the five cycles of filtration and Fenton cleaning, presented a very small defect percentage (<5%), comparable to the percentage of its initial defects (about 4%), suggesting a minimal or no effect of Fenton cleaning on the membrane integrity. As observed in
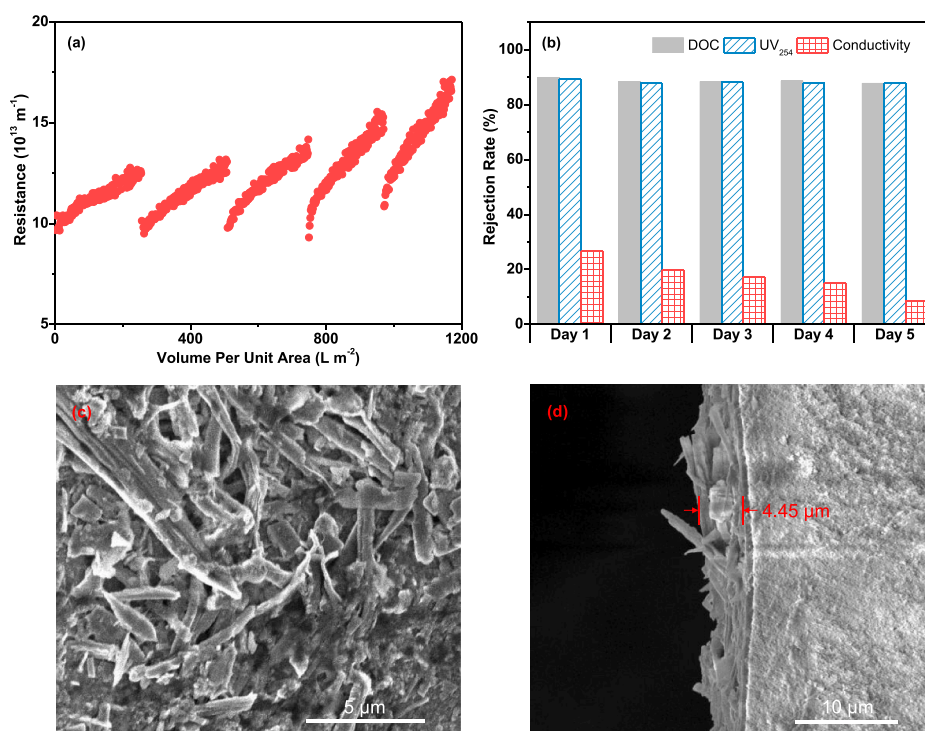

Fig. 8. (a) Direct canal water filtration using FeOCl pre-coated membrane at a constant-pressure of 3.0 bar with periodical Fenton cleaning over five cycles (1 d for each cycle). The FeOCl pre-coat layer and H$_2$O$_2$ solution were not renewed between the cycles. (b) Variations in rejection performance of the membrane over dissolved organic carbon (DOC), ultraviolet absorbance at 254 nm (UV$_{254}$) and conductivity during five-day filtration. (c) Top-view and (d) cross-sectional SEM images of the membrane after five one-day filtration and cleaning cycles.

Fig. 8c and d, the membrane surface after the fifth cycle was still covered with the FeOCl pre-coat layer with a thickness of approximately 4.5 μm, compared to the initial thickness of 5.3 μm (Fig. 3e, Section 3.1). The aforementioned results, collectively, validate the good stability and reactivity of the FeOCl pre-coat layer on the ceramic NF membrane during its long-term repeated uses for direct filtration of surface (canal) water and Fenton cleaning.

4. Conclusions

A structural and functional design of the surface of ceramic NF membranes, in response to combined NOM and colloid fouling, is of practical significance for their direct surface water treatment applications. In this study, a catalytic layer, consisting of an active FeOCl catalyst, was pre-coated on top of commercial ceramic NF membranes, for segregating a large-sized colloid fraction in canal water from the TiO_2 separation layer and Fenton cleaning.

The main conclusions of the study were:

(1) The catalyst pre-coat layer, having a much larger pore size (0.1−0.5 μm) than the TiO_2 separation layer of the membrane (0.9 nm), only led to a minimal permeance decrease of the membrane (<4%).
(2) The large-sized colloid fraction (3−30 μm) in the canal water was identified as a paramount substance fouling the separation layer of the pristine membrane. The catalyst pre-coat layer on the membrane was able to segregate the large-sized colloid fraction from the separation layer at an acceptable flux of about 23 L m^{-2} h^{-1}, without causing pronounced clogging within its pores.
(3) The catalytic pre-coat layer facilitated the restoration of the filtration resistance through Fenton cleaning, while the separation layer of the membrane maintained a high rejection of the NOM (approximately 90%) over five one-day filtration and cleaning cycles.
(4) The pre-coat layer remained reproducible over the five long-running cycles, having only a minor loss of 15.6% in its thickness.

CRediT authorship contribution statement

Bin Lin: Conceptualization, Data curation, Investigation, Methodology, Writing – original draft, Writing – review & editing. **Sebastiaan G.J. Heijman:** Conceptualization, Methodology, Supervision, Writing – review & editing. **Luuk C. Rietveld:** Supervision, Writing – review & editing.

Declaration of competing interest

The authors declare that they have no known competing financial interests or personal relationships that could have appeared to influence the work reported in this paper.

Data availability

Data will be made available on request.

Acknowledgement

Appendix A. Supplementary data

Supplementary data to this article can be found online at https://doi.org/10.1016/j.memsci.2023.122401.

References

[1] L. Ho, K. Braun, R. Fabris, D. Hoefel, J. Morran, P. Monis, M. Drikas, Comparison of drinking water treatment process streams for optimal bacteriological water quality, Water Res. 46 (2012) 3934–3942, https://doi.org/10.1016/j.watres.2012.04.041.

[2] S.J. Köhler, E. Lavonen, A. Keucken, P. Schmitt-Kopplin, T. Spanjer, K. Persson, Upgrading coagulation with hollow-fibre nanofiltration for improved organic matter removal during surface water treatment, Water Res. 89 (2016) 232–240, https://doi.org/10.1016/j.watres.2015.11.048.

[3] H. Futselaar, H. Schonewille, W. van der Meer, Direct capillary nanofiltration – a new high-grade purification concept, Desalination 145 (2002) 75–80, https://doi.org/10.1016/S0011-9164(02)00389-2.

[4] C. Dreszer, H.C. Flemming, A. Zwijnenburg, J.C. Kruithof, J.S. Vrouwenvelder, Impact of biofilm accumulation on transmembrane and feed channel pressure drop: effects of crossflow velocity, feed spacer and biodegradable nutrient, Water Res. 50 (2014) 200–211, https://doi.org/10.1016/j.watres.2013.11.024.

[5] Y. Wibisono, W. Yandi, M. Golabi, R. Nugraha, Emile R. Cornelissen, A.J.B. Kemperman, T. Ederth, K. Nijmeijer, Hydrogel-coated feed spacers in two-phase flow cleaning in spiral wound membrane elements: a novel platform for eco-friendly biofouling mitigation, Water Res. 71 (2015) 171–186, https://doi.org/10.1016/j.watres.2014.12.030.

[6] T. Fujioka, M.T.T. Ngo, R. Makabe, T. Ueyama, H. Takeuchi, T.T.V. Nga, X.-T. Bui, H. Tanaka, Submerged nanofiltration without pre-treatment for direct advanced drinking water treatment, Chemosphere 265 (2021) 129056, https://doi.org/10.1016/j.chemosphere.2020.129056.

[7] Y.-y. Zhao, X.-m. Wang, H.-w. Yang, Y.-f.F. Xie, Effects of organic fouling and cleaning on the retention of pharmaceutically active compounds by ceramic nanofiltration membranes, J. Membr. Sci. 563 (2018) 734–742, https://doi.org/10.1016/j.memsci.2018.06.047.

[8] S. Li, H. Meng, H. Wang, J.S. Vrouwenvelder, Z. Li, A sacrificial protective layer as fouling control strategy for nanofiltration in water treatment, Water Res. 219 (2022) 118554, https://doi.org/10.1016/j.watres.2022.118554.

[9] J. Shim, S. Park, K.H. Cho, Deep learning model for simulating influence of natural organic matter in nanofiltration, Water Res. 197 (2021) 117070, https://doi.org/10.1016/j.watres.2021.117070.

[10] A.R.D. Verliefde, E.R. Cornelissen, S.G.J. Heijman, I. Petrinic, T. Luxbacher, G. L. Amy, B. Van der Bruggen, J.C. van Dijk, Influence of membrane fouling by (pretreated) surface water on rejection of pharmaceutically active compounds (PhACs) by nanofiltration membranes, J. Membr. Sci. 330 (2009) 90–103, https://doi.org/10.1016/j.memsci.2008.12.039.

[11] X. Guo, Q. Li, W. Hu, W. Gao, D. Liu, Ultrafiltration of dissolved organic matter in surface water by a polyvinylchloride hollow fiber membrane, J. Membr. Sci. 327 (2009) 254–263, https://doi.org/10.1016/j.memsci.2008.11.042.

[12] Y. Kim, M. Elimelech, H.K. Shon, S. Hong, Combined organic and colloidal fouling in forward osmosis: fouling reversibility and the role of applied pressure, J. Membr. Sci. 460 (2014) 206–212, https://doi.org/10.1016/j.memsci.2014.02.038.

[13] Q. Li, M. Elimelech, Synergistic effects in combined fouling of a loose nanofiltration membrane by colloidal materials and natural organic matter, J. Membr. Sci. 278 (2006) 72–82, https://doi.org/10.1016/j.memsci.2005.10.045.

[14] T.O. Mahlangu, E.M.V. Hoek, B.B. Mamba, A.R.D. Verliefde, Influence of organic, colloidal and combined fouling on NF rejection of NaCl and carbamazepine: role of solute–foulant–membrane interactions and cake-enhanced concentration polarisation, J. Membr. Sci. 471 (2014) 35–46, https://doi.org/10.1016/j.memsci.2014.07.065.

[15] S. Lee, J. Cho, M. Elimelech, Combined influence of natural organic matter (NOM) and colloidal particles on nanofiltration membrane fouling, J. Membr. Sci. 262 (2005) 27–41, https://doi.org/10.1016/j.memsci.2005.03.043.

[16] G. Mustafa, K. Wyns, A. Buekenhoudt, V. Meynen, New insights into the fouling mechanism of dissolved organic matter applying nanofiltration membranes with a variety of surface chemistries, Water Res. 93 (2016) 195–204, https://doi.org/10.1016/j.watres.2016.02.030.

[17] G. Mustafa, K. Wyns, P. Vandezande, A. Buekenhoudt, V. Meynen, Novel grafting method efficiently decreases irreversible fouling of ceramic nanofiltration membranes, J. Membr. Sci. 470 (2014) 369–377, https://doi.org/10.1016/j.memsci.2014.07.050.

[18] B. Lin, S.G.J. Heijman, R. Shang, L.C. Rietveld, Integration of oxalic acid chelation and Fenton process for synergistic relaxation-oxidation of persistent gel-like fouling of ceramic nanofiltration membranes, J. Membr. Sci. 636 (2021) 119553, https://doi.org/10.1016/j.memsci.2021.119553.

[19] F.C. Kramer, R. Shang, L.C. Rietveld, S.J.G. Heijman, Fouling control in ceramic nanofiltration membranes during municipal sewage treatment, Sep. Purif. Technol. 237 (2020) 116373, https://doi.org/10.1016/j.seppur.2019.116373.

[20] F.C. Kramer, R. Shang, S.M. Scherrenberg, L.C. Rietveld, S.J.G. Heijman, Quantifying defects in ceramic tight ultra- and nanofiltration membranes and investigating their robustness, Sep. Purif. Technol. 219 (2019) 159–168, https://doi.org/10.1016/j.seppur.2019.03.019.

[21] N. Zhang, Q. Li, C. Li, Z. Li, L. Zhao, X. Zhang, Y. Wang, Z. Li, X. Dou, W. Cui, S. Li, Highly ordered mesostructured flexible silica-based nanofiltration membrane with satisfactory acid, chlorine, and fouling resistances, J. Membr. Sci. 678 (2023) 121635, https://doi.org/10.1016/j.memsci.2023.121635.

[22] S.S. Wadekar, R.D. Vidic, Comparison of ceramic and polymeric nanofiltration membranes for treatment of abandoned coal mine drainage, Desalination 440 (2018) 135–145, https://doi.org/10.1016/j.desal.2018.01.008.

[23] S. Sun, H. Yao, W. Fu, L. Hua, G. Zhang, W. Zhang, Reactive Photo-Fenton ceramic membranes: synthesis, characterization and antifouling performance, Water Res. 144 (2018) 690–698, https://doi.org/10.1016/j.watres.2018.08.002.

[24] L. Zhu, W. Wang, P. Zhao, S. Wang, K. Yang, H. Shi, M. Xu, Y. Dong, Silicon carbide catalytic ceramic membranes with nano-wire structure for enhanced anti-fouling performance, Water Res. 226 (2022) 119209, https://doi.org/10.1016/j.watres.2022.119209.

[25] X. Wang, Y. Li, H. Yu, F. Yang, C.Y. Tang, X. Quan, Y. Dong, High-flux robust ceramic membranes functionally decorated with nano-catalyst for emerging micro-pollutant removal from water, J. Membr. Sci. 611 (2020) 118281, https://doi.org/10.1016/j.memsci.2020.118281.

[26] Y. He, L. Wang, Z. Chen, X. Huang, X. Wang, X. Zhang, X. Wen, Novel catalytic ceramic membranes anchored with MnMe oxide and their catalytic ozonation performance towards atrazine degradation, J. Membr. Sci. 648 (2022) 120362, https://doi.org/10.1016/j.memsci.2022.120362.

[27] T.E. Berger, C. Regmi, A.I. Schäfer, B.S. Richards, Photocatalytic degradation of organic dye via atomic layer deposited TiO₂ on ceramic membranes in single-pass flow-through operation, J. Membr. Sci. 604 (2020) 118015, https://doi.org/10.1016/j.memsci.2020.118015.

[28] L. De Angelis, M.M.F. de Cortalezzi, Improved membrane flux recovery by Fenton-type reactions, J. Membr. Sci. 500 (2016) 255–264, https://doi.org/10.1016/j.memsci.2015.11.042.

[29] S.A. Heredia Deba, B.A. Wols, D.R. Yntema, R.G.H. Lammertink, Advanced ceramics in radical filtration: TiO₂ layer thickness effect on the photocatalytic membrane performance, J. Membr. Sci. 672 (2023) 121423, https://doi.org/10.1016/j.memsci.2023.121423.

[30] B. Lin, L.C. Rietveld, L. Yao, S.G.J. Heijman, Adsorption and cake layer fouling in relation to Fenton cleaning of ceramic nanofiltration membranes, J. Membr. Sci. 687 (2023) 122097, https://doi.org/10.1016/j.memsci.2023.122097.

[31] Z. Bai, S. Gao, H. Yu, X. Liu, J. Tian, Layered metal oxides loaded ceramic membrane activating peroxymonosulfate for mitigation of NOM membrane fouling, Water Res. 222 (2022) 118928, https://doi.org/10.1016/j.watres.2022.118928.

[32] Z. Bai, S. Gao, X. Liu, R. Huang, J. Tian, Ceramic membrane with double catalytic layer for efficient peroxymonosulfate activation and dissolved organic matter (DOM) membrane fouling control, Sep. Purif. Technol. 318 (2023) 123999, https://doi.org/10.1016/j.seppur.2023.123999.

[33] Y. Chen, C.J. Miller, R.N. Collins, T.D. Waite, Key considerations when assessing novel Fenton catalysts: iron oxychloride (FeOCl) as a case study, Environ. Sci. Technol. 55 (2021) 13317–13325, https://doi.org/10.1021/acs.est.1c04370.

[34] X.-J. Yang, X.-M. Xu, J. Xu, Y.-F. Han, Iron oxychloride (FeOCl): an efficient Fenton-like catalyst for producing hydroxyl radicals in degradation of organic contaminants, J. Am. Chem. Soc. 135 (2013), https://doi.org/10.1021/ja409130c, 16058–16061.

[35] M. Sun, C. Chu, F. Geng, X. Lu, J. Qu, J. Crittenden, M. Elimelech, J.-H. Kim, Reinventing Fenton chemistry: iron oxychloride nanosheet for pH-insensitive H₂O₂ activation, Environ. Sci. Technol. Lett. 5 (2018) 186–191, https://doi.org/10.1021/acs.estlett.8b00065.

[36] H. Futselaar, H. Schonewille, W. van der Meer, Direct capillary nanofiltration for surface water, Desalination 157 (2003) 135–136, https://doi.org/10.1016/S0011-9164(03)00392-8.

[37] J. Kim, W. Shan, S.H.R. Davies, M.J. Baumann, S.J. Masten, V.V. Tarabara, Interactions of aqueous NOM with nanoscale TiO₂: implications for ceramic membrane filtration-ozonation hybrid process, Environ. Sci. Technol. 43 (2009) 5488–5494, https://doi.org/10.1021/es900342q.

[38] M.A. Sari, S. Chellam, Relative contributions of organic and inorganic fouling during nanofiltration of inland brackish surface water, J. Membr. Sci. 523 (2017) 68–76, https://doi.org/10.1016/j.memsci.2016.10.005.

[39] K. Tominaga, R. Nagai, A. Hafuka, W. Yu, K. Kimura, Isolation of LC-OCD-quantified biopolymers from surface water: significant differences between real biopolymers and model biopolymers, J. Membr. Sci. 658 (2022) 120714, https://doi.org/10.1016/j.memsci.2022.120714.

[40] L. Xu, C. Wei, M.S. Siddique, W. Yu, Insight into the effect of in-situ galvanic micro-coagulation on membrane fouling mitigation treating surface water, J. Membr. Sci. 610 (2020) 118234, https://doi.org/10.1016/j.memsci.2020.118234.

[41] D.J. Miller, S. Kasemset, D.R. Paul, B.D. Freeman, Comparison of membrane fouling at constant flux and constant transmembrane pressure conditions, J. Membr. Sci. 454 (2014) 505–515, https://doi.org/10.1016/j.memsci.2013.12.027.

[42] K.-H. Choo, C.-H. Lee, Membrane fouling mechanisms in the membrane-coupled anaerobic bioreactor, Water Res. 30 (1996) 1771–1780, https://doi.org/10.1016/0043-1354(96)00053-X.

[43] A.Y. Kirschner, Y.-H. Cheng, D.R. Paul, R.W. Field, B.D. Freeman, Fouling mechanisms in constant flux crossflow ultrafiltration, J. Membr. Sci. 574 (2019) 65–75, https://doi.org/10.1016/j.memsci.2018.12.001.

[44] R. Shang, A. Goulas, C.Y. Tang, X. de Frias Serra, L.C. Rietveld, S.G.J. Heijman, Atmospheric pressure atomic layer deposition for tight ceramic nanofiltration membranes: synthesis and application in water purification, J. Membr. Sci. 528 (2017) 163–170, https://doi.org/10.1016/j.memsci.2017.01.023.

[45] I. Caltran, L.C. Rietveld, H.L. Shorney-Darby, S.G.J. Heijman, Separating NOM from salts in ion exchange brine with ceramic nanofiltration, Water Res. 179 (2020) 115894, https://doi.org/10.1016/j.watres.2020.115894.

[46] H. Xu, M. Xu, Y. Li, X. Liu, L. Guo, H. Jiang, Characterization, origin and aggregation behavior of colloids in eutrophic shallow lake, Water Res. 142 (2018) 176–186, https://doi.org/10.1016/j.watres.2018.05.059.

[47] D. Li, W. Lin, R. Shao, Y.-X. Shen, X. Zhu, X. Huang, Interaction between humic acid and silica in reverse osmosis membrane fouling process: a spectroscopic and molecular dynamics insight, Water Res. 206 (2021) 117773, https://doi.org/10.1016/j.watres.2021.117773.

[48] Y. Zhao, R. Kitajima, N. Shirasaki, Y. Matsui, T. Matsushita, Precoating membranes with submicron super-fine powdered activated carbon after coagulation prevents transmembrane pressure rise: straining and high adsorption capacity effects, Water Res. 177 (2020) 115757, https://doi.org/10.1016/j.watres.2020.115757.

[49] B. Malczewska, J. Liu, M.M. Benjamin, Virtual elimination of MF and UF fouling by adsorptive pre-coat filtration, J. Membr. Sci. 479 (2015) 159–164, https://doi.org/10.1016/j.memsci.2015.01.032.

[50] G. Mustafa, K. Wyns, A. Buekenhoudt, V. Meynen, Antifouling grafting of ceramic membranes validated in a variety of challenging wastewaters, Water Res. 104 (2016) 242–253, https://doi.org/10.1016/j.watres.2016.07.057.

[51] Y. So, Y. Lee, S. Kim, J. Lee, C. Park, Role of co-existing ions in the removal of dissolved silica by ceramic nanofiltration membrane, J. Water Process Eng. 53 (2023) 103873, https://doi.org/10.1016/j.jwpe.2023.103873.

[52] A. Anantharaman, Y. Chun, T. Hua, J.W. Chew, R. Wang, Pre-deposited dynamic membrane filtration – a review, Water Res. 173 (2020) 115558, https://doi.org/10.1016/j.watres.2020.115558.

[53] J. Luo, M. Sun, C.L. Ritt, X. Liu, Y. Pei, J.C. Crittenden, M. Elimelech, Tuning Pb(II) adsorption from aqueous solutions on ultrathin iron oxychloride (FeOCl) nanosheets, Environ. Sci. Technol. 53 (2019) 2075–2085, https://doi.org/10.1021/acs.est.8b07027.

[54] P. Yao, K.-H. Choo, M.-H. Kim, A hybridized photocatalysis–microfiltration system with iron oxide-coated membranes for the removal of natural organic matter in water treatment: effects of iron oxide layers and colloids, Water Res. 43 (2009) 4238–4248, https://doi.org/10.1016/j.watres.2009.06.010.

[55] J.F. Soesanto, K.-J. Hwang, C.-W. Cheng, H.-Y. Tsai, A. Huang, C.-H. Chen, T.-W. Cheng, K.-L. Tung, Fenton oxidation-based cleaning technology for powdered activated carbon-precoated dynamic membranes used in microfiltration seawater pretreatment systems, J. Membr. Sci. 591 (2019) 117298, https://doi.org/10.1016/j.memsci.2019.117298.

[56] J. Shao, J. Hou, H. Song, Comparison of humic acid rejection and flux decline during filtration with negatively charged and uncharged ultrafiltration membranes, Water Res. 45 (2011) 473–482, https://doi.org/10.1016/j.watres.2010.09.006.

[57] M.A. Zazouli, H. Susanto, S. Nasseri, M. Ulbricht, Influences of solution chemistry and polymeric natural organic matter on the removal of aquatic pharmaceutical residuals by nanofiltration, Water Res. 43 (2009) 3270–3280, https://doi.org/10.1016/j.watres.2009.04.038.

[58] S. Ognier, C. Wisniewski, A. Grasmick, Membrane bioreactor fouling in sub-critical filtration conditions: a local critical flux concept, J. Membr. Sci. 229 (2004) 171–177, https://doi.org/10.1016/j.memsci.2003.10.026.

[59] Y. Ninomiya, K. Kimura, T. Sato, T. Kakuda, M. Kaneda, A. Hafuka, T. Tsuchiya, High-flux operation of MBRs with ceramic flat-sheet membranes made possible by intensive membrane cleaning: tests with real domestic wastewater under low-temperature conditions, Water Res. 181 (2020) 115881, https://doi.org/10.1016/j.watres.2020.115881.

[60] P. Árki, C. Hecker, G. Tomandl, Y. Joseph, Streaming potential properties of ceramic nanofiltration membranes – importance of surface charge on the ion rejection, Sep. Purif. Technol. 212 (2019) 660–669, https://doi.org/10.1016/j.seppur.2018.11.054.

[61] F.C. Kramer, R. Shang, L.C. Rietveld, S.J.G. Heijman, Influence of pH, multivalent counter ions, and membrane fouling on phosphate retention during ceramic nanofiltration, Sep. Purif. Technol. 227 (2019) 115675, https://doi.org/10.1016/j.seppur.2019.115675.

[62] F.H. Kamil, M.Y. Hussein, A.N.A. Al-Naemi, A.F. Al-Alawy, Measuring zeta potential of ceramic TiO₂ NF membrane for different salts by filtration potential technique using innovated silver electrodes, Desalination Water Treat. 160 (2019) 71–80, https://doi.org/10.5004/dwt.2019.24372.